SCIENCE CHINA
Physics, Mechanics & Astronomy

• Article •

April 2012 Vol.55 No.4: 684–692
doi: 10.1007/s11433-012-4663-3

Instability of thermocapillary flow in liquid layers under microgravity†

XUN Bo, LI Kai & HU WenRui*

Key Laboratory of Microgravity (National Microgravity Laboratory), Institute of Mechanics, Chinese Academy of Sciences, Beijing 100190, China

Received January 9, 2012; accepted February 6, 2012; published online March 8, 2012

The instability of the thermocapillary flow in liquid layers is studied in the present paper using the linear stability analysis. Based on the two-dimensional steady flow state, the three-dimensional disturbance with a wave number in the spanwise direction is considered. The effects of the aspect ratio and free surface shape of the liquid layer on the flow instability are studied, and the results are compared with the case with the two-dimensional disturbance.

thermocapillary convection, flow instability, numerical simulations of chaotic systems

PACS number(s): 47.55.nb, 47.20.Ky, 05.45.Pq

Citation: Xun B, Li K, Hu W R. Instability of thermocapillary flow in liquid layers under microgravity. Sci China-Phys Mech Astron, 2012, 55: 684–692, doi: 10.1007/s11433-012-4663-3

Instability of thermocapillary flow in liquid layers has received considerable attention [1,2]. Smith et al. conducted a linear stability analysis for thermocapillary flow in liquid layers of infinite extension and revealed the hydrothermal wave instability which is a pair of obliquely traveling wave toward the hot region [3]. The corresponding instability mechanism was also studied [3,4]. Smith further studied the slightly supercritical nonlinear behavior and found that possible waveforms are composed of only one of the unstable linear waves for all Prandtl numbers and small Biot numbers [5]. For liquid layers of finite extension, there are a bunch of two-dimensional theoretical and numerical studies. Strani et al. [6] developed an asymptotic theory in the limiting case where the aspect ratio tends to infinity and numerically studied the steady thermocapillary flow in finite rectangular cavities. Carpenter et al. studied the steady thermocapillary flow in a square cavity for different Prandtl numbers, and they also did a linear stability analysis but found no instability [7]. A time-dependent numerical simulation was made by Peltier et al. and a stability diagram of the critical Marangoni number versus the aspect ratio was given [8]. There are also a couple of three-dimensional numerical simulations, e.g., the steady thermocapillary flow in a cubic container was studied, and the flow and temperature field structures were provided [9–11] which exhibit dramatic complexity compared with the two-dimensional case. Xu et al. [12] studied the two- and three-dimensional thermocapillary flow and the corresponding instability by numerical simulation. They pointed out that sidewalls have a damping effect on the flow oscillations and hence increase the critical Reynolds number. However, the existence of spanwise waves can reduce the critical Reynolds number.

In the present paper, we conducted the linear stability analysis on two-dimensional liquid layers with infinite extension in the spanwise direction as used by Schimmel et al. [13]. Although the basic flow field is still two-dimensional, the three-dimensional disturbances with a wave number in the spanwise direction were considered. With this approach, the spanwise waves arising in a three-dimensional system

*Corresponding author (email: wrhu@imech.ac.cn)
†Recommended by Hu WenRui (CAS Academician)

can be studied but the complexity of three-dimensional numerical simulation can be avoided. The effects of the aspect ratio and the free surface shape of the liquid layer on the instability of the steady basic flow state are the focus of the present linear stability analysis.

1 Governing equations and numerical scheme

Figure 1 shows a schematic diagram of a 2D liquid layer of 1cst silicone oil (Pr=16.1). The thickness of the liquid layer at the sidewall is H and the extension is L. The contact angle at the end wall is β. The temperatures at the hot end (left) and cold end (right) of the liquid layer are T_H and T_C respectively. The bottom plate and free surface are both adiabatic. The length, velocity, pressure and time are scaled by H, $\frac{\gamma\Delta TH}{\mu L}$, $\frac{\gamma\Delta T}{L}$ and $\frac{H^2}{\upsilon}$, respectively. The temperature measured with respect to $\frac{(T_H+T_C)}{2}$ is scaled by $\Delta T = (T_H - T_C)$. The non-dimensional governing equations are as follows:

$$\nabla\cdot\boldsymbol{U}=0. \tag{1}$$

$$\frac{\partial\boldsymbol{U}}{\partial t}+Re(\boldsymbol{U}\cdot\nabla)\boldsymbol{U}+\nabla P=\Delta\boldsymbol{U}, \tag{2}$$

$$\frac{\partial T}{\partial t}+Re(\boldsymbol{U}\cdot\nabla)T=\frac{1}{Pr}\Delta T, \tag{3}$$

where $\boldsymbol{U}$, P and T are the velocity vector, pressure and temperature, and the dimensionless parameters $Pr=\frac{\upsilon}{\alpha}$ and $Re=\frac{\gamma\Delta TH^2}{\mu\upsilon L}$ are Prandtl number and Reynolds number respectively. The corresponding boundary conditions are

$$x=0,\ \Gamma:\quad \boldsymbol{U}=0,\ T=\pm\frac{1}{2}, \tag{4}$$

$$z=0:\quad \boldsymbol{U}=0,\ \frac{\partial T}{\partial z}=0, \tag{5}$$

$$\begin{aligned} &z=h(x):\quad \boldsymbol{n}\cdot\boldsymbol{U}=0,\ \boldsymbol{t}_x\cdot(S\bullet\boldsymbol{n})=-\boldsymbol{t}_x\cdot\nabla T,\\ &\boldsymbol{t}_y\cdot(S\cdot\boldsymbol{n})=-\boldsymbol{t}_y\cdot\nabla T,\ \boldsymbol{n}\cdot\nabla T=0, \end{aligned} \tag{6}$$

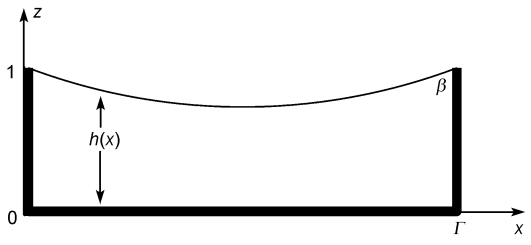

Figure 1 Schematic sketch of a two-dimensional liquid layer.

where $\Gamma=L/H$ is the aspect ratio, $h(x)$ is the vertical position of the free surface, $\boldsymbol{n}$ is the normal vector of the free surface, $\boldsymbol{t}_x$ and $\boldsymbol{t}_y$ are the tangential vectors of the free surface in the (x, z) plane and the (y, z) plane respectively.

For the linear stability analysis, the basic two-dimensional steady state:

$$X=\{\boldsymbol{U}(x,z)=U\boldsymbol{e}_x+W\boldsymbol{e}_z,\ P(x,z),\ T(x,z)\}$$

is first determined for a given set of parameters (Re, Pr, β and Γ). Then small three-dimensional disturbances are imposed on the basic state, and the corresponding equations are linearized by neglecting high orders of the disturbances. The disturbances are assumed to be in the normal mode:

$$\begin{pmatrix}\boldsymbol{u}'\\ p'\\ T'\end{pmatrix}=\sum_{m=-\infty}^{+\infty}\begin{pmatrix}\boldsymbol{u}'^m(x,z)\\ p'^m(x,z)\\ T'^m(x,z)\end{pmatrix}\exp[\sigma^{(m)}t+\mathrm{i}my], \tag{7}$$

where m is the wave number in the spanwise direction.

The linearized disturbance equations are as follows:

$$u'_x+w'_z+imv'=0, \tag{8}$$

$$\begin{aligned} &Re(Uu'_x+Wu'_z+U_xu'+U_zw')+p'_x\\ &-u'_{xx}-u'_{zz}+m^2u'=-\sigma^{(m)}u'. \end{aligned} \tag{9}$$

$$Re(Uv'_x+Wv'_z)+imp-v'_{xx}-v'_{zz}+m^2v'=-\sigma^{(m)}v', \tag{10}$$

$$\begin{aligned} &Re(Uw'_x+Ww'_z+W_xu'+W_zw')+p'_z-w'_{xx}-w'_{zz}+m^2w'\\ &=-\sigma^{(m)}w', \end{aligned} \tag{11}$$

$$\begin{aligned} &Re(UT'_x+WT'_z+u'T_x+w'T_z)\\ &-\frac{1}{\mathrm{Pr}}(T'_{xx}+T'_{zz}-m^2T')=-\sigma^{(m)}T'. \end{aligned} \tag{12}$$

The corresponding boundary conditions are:

$$\begin{aligned} &x=0,\ \Gamma:\\ &\boldsymbol{u}'=0,\ T'=0, \end{aligned} \tag{13}$$

$$\begin{aligned} &z=0:\\ &\boldsymbol{u}'=0,\ \frac{\partial T'}{\partial z}=0, \end{aligned} \tag{14}$$

$$\begin{aligned} &z=h(x):\\ &\boldsymbol{n}\cdot\boldsymbol{u}'=0,\ \boldsymbol{t}_x\cdot(s\cdot\boldsymbol{n})=-\boldsymbol{t}_x\cdot\nabla T,\\ &\boldsymbol{t}_y\cdot(s\cdot\boldsymbol{n})=-\boldsymbol{t}_y\cdot\nabla T,\ \boldsymbol{n}\cdot\nabla T'=0. \end{aligned} \tag{15}$$

For curved free surface liquid layers, a curve-fitting coordinate is generated by an algebra transformation:

$$\begin{cases}\xi=x,\\ \eta=\dfrac{z}{h(x)}.\end{cases} \tag{16}$$

With this transformation, the previous equations are

transformed from the curved physical domain ($0 \leqslant x \leqslant \Gamma$, $0 \leqslant z \leqslant h(x)$) into the rectangular calculating domain ($0 \leqslant \xi \leqslant \Gamma$, $0 \leqslant \eta \leqslant 1$).

The discrete form of the linearized equations can be written as a generalized eigenvalue problem:

$$g(x,\ X,\ Re,\ m,\ Pr,\ \Gamma,\ \beta) \equiv Ax = Bx, \tag{17}$$

where

$$x = \{u'(x,z), iv'(x,z), w'(x,z),\ p'(x,z), T'(x,z)\} \tag{18}$$

is the disturbance vector. The eigenvalues and the related eigenvectors of the problem are solved by the Arnoldi method [14]. The critical Reynolds number (Re_c) is obtained when the maximum of the real part of $\sigma(m)$ for all m is zero, and the disturbance frequency is the imaginary part of $\sigma(m)$. Accordingly, the critical Reynolds number corresponding to two-dimensional disturbances (m=0) is indicated as Re_{c0}. In order to well resolve the boundary layers at both ends, a non-uniform mesh with denser grid points near both solid ends and free surface is adopted in this study. A code validation for the thermocapillary convection in a square cavity is shown in Table 1.

2 Results and discussions

2.1 Flat free surface (β=90°)

Figures 2 and 3 show the streamlines and isothermals of the two-dimensional steady basic flow state in liquid layers with flat free surface at the critical states. For the liquid

Table 1 Code validation for thermocapillary convection in a square cavity

Pr	*Re*	ψ_{min} ($\times 10^3$)	ω_{core} ($\times 10^2$)	
1	10000	–3.22	–7.00	Present paper
		–3.21	–7.01	Xu et al. [10]
30	2000	–1.59	–6.01	Present paper
		–1.69	–6.27	Xu et al. [10]

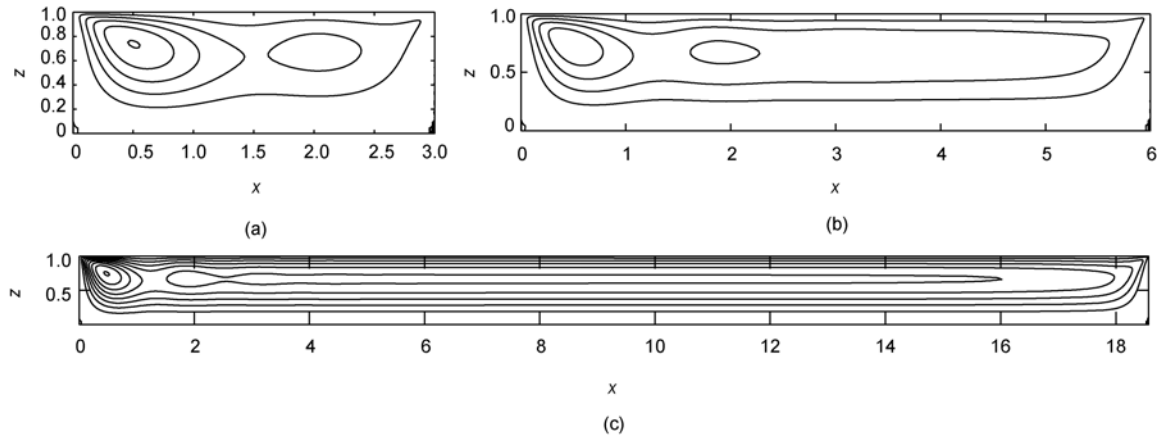

Figure 2 Streamlines of the two-dimensional steady basic flow state at the corresponding critical Reynolds number. (a) Γ=3, Re_c=264; (b) Γ=6, Re_c=82; (c) Γ=18.6, Re_c=37.

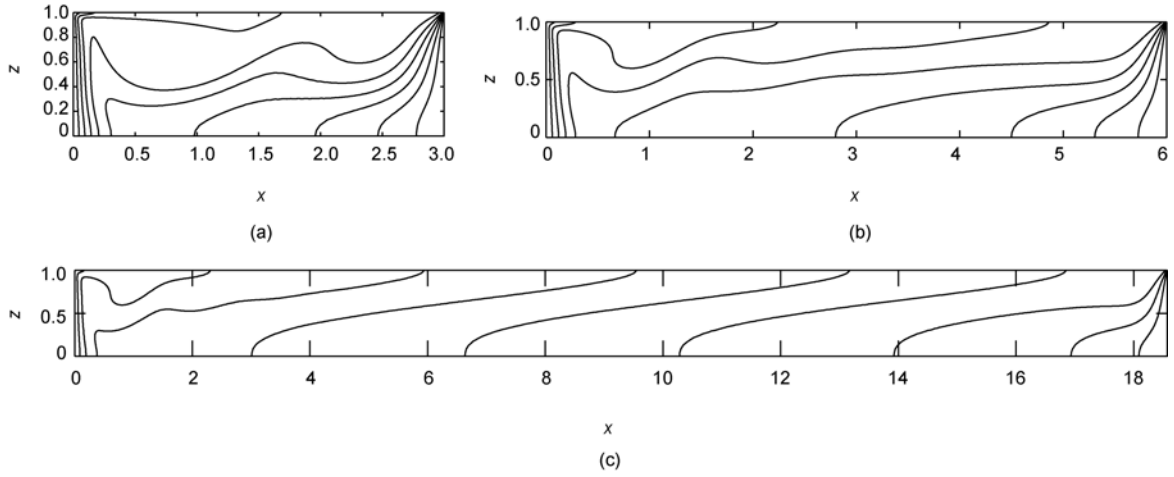

Figure 3 Isothermals of the two-dimensional steady basic flow state at the corresponding critical Reynolds number. (a) Γ=3, Re_c=264; (b) Γ=6, Re_c=82; (c) Γ=18.6, Re_c=37.

layers of different aspect ratios, a strong vortex always occurs near the hot end with the vortex center approximately located at z=2/3. There is also a weaker vortex in the bulk of the liquid layers which laterally elongates with the increasing aspect ratio. For the large aspect-ratio liquid layers, Γ=18.6 for instance, the flow in the central region of the liquid layers is similar to the plane-parallel flow with nearly homogenous temperature gradient.

Table 2 shows the critical Reynolds number, wave number and frequency versus the aspect ratio for the liquid layers with flat free surface where the mesh size $N_z \times N_x$ indicates the number of grid points used in the z direction (N_z) and x direction (N_x). The Re_c slightly increases with the decreasing aspect ratio in the range of large aspect ratios and then increases sharply in the range of small aspect ratios (see Figure 4). On the other hand, the critical wave number and frequency only slightly varies in the aspect-ratio range studied. Figures 5 and 6 show the distributions of the

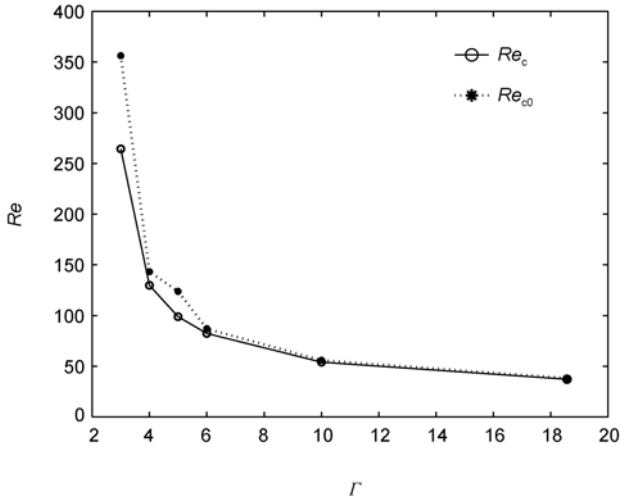

Figure 4 Critical Reynolds number versus aspect ratio for liquid layers with a flat free surface.

Table 2 Critical Reynolds number versus aspect ratio for liquid layers with a flat free surface

Γ	Mesh size	Re_c	m_c	f_c	Re_{c0}	f_{c0}
3	51×201	264	0.9	3.01	356	10.2
4	51×201	130	0.9	2.85	143	2.56
5	51×301	99	1.1	3.03	124	2.75
6	61×351	82	1.1	3.05	87	2.77
10	51×501	54	1	3.04	56	2.86
18.6	51×751	37	1	3.06	38	2.89

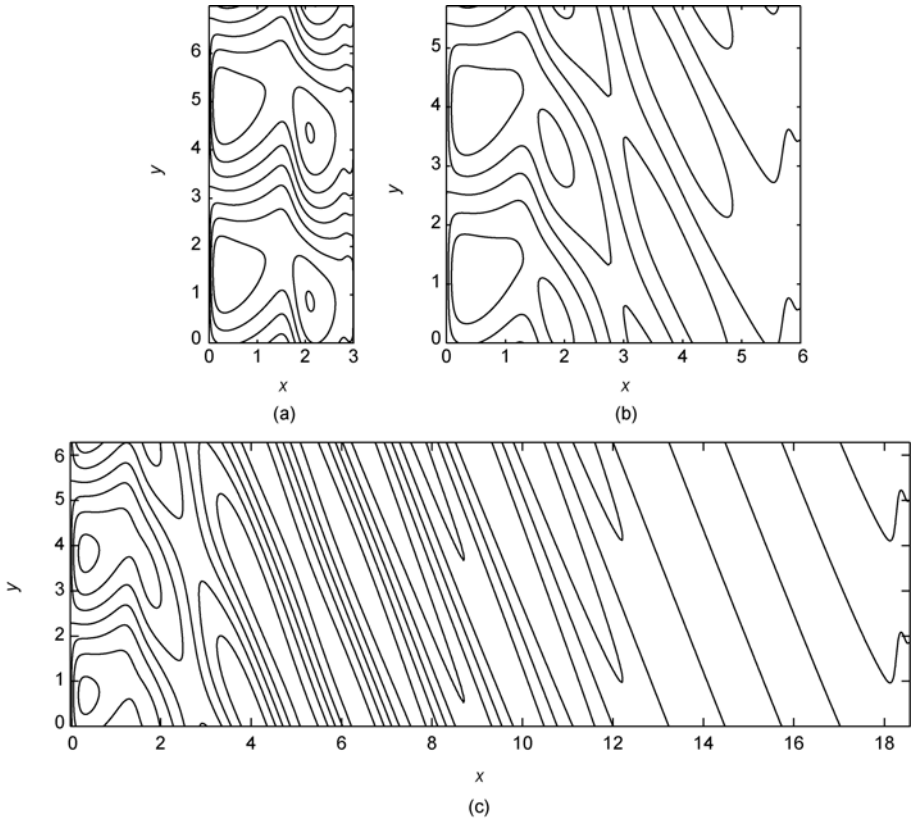

Figure 5 Critical temperature disturbance distribution on the free surface. (a) Γ=3, Re_c=264; (b) Γ=6, Re_c=82; (c) Γ=18.6, Re_c=37.

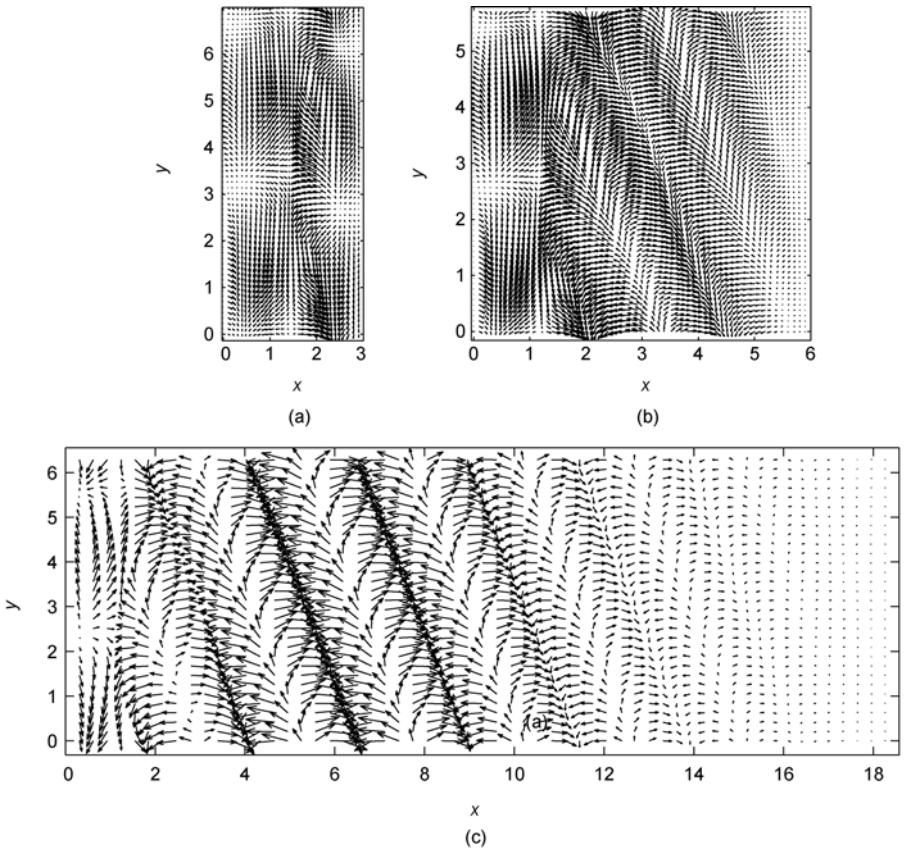

Figure 6 Critical velocity disturbance distribution on the free surface. (a) Γ=3, Re_c=264; (b) Γ=6, Re_c=82; (c) Γ=18.6, Re_c=37.

three-dimensional critical temperature and velocity disturbances on the free surface of the liquid layers of different aspect ratios. For the large aspect-ratio liquid layers, Γ=18.6 for instance, the disturbance near the cold end is much weaker than that in the rest region. For the liquid layers of intermediate and small aspect ratios, however, the disturbance develops in the whole liquid region. For the small aspect-ratio liquid layers, Γ=3 for instance, the three-dimensional disturbance is a traveling wave in the spanwise direction. With the increasing Γ, the three-dimensional disturbance behaves in a more complex way. It behaves as a traveling wave in the spanwise direction near the hot end. In the remaining region, however, it behaves as an obliquely traveling wave from the cold region to the hot region, and the angle between the traveling direction of the wave and the negative x direction is small (about 20 degrees seen from Figures 5 and 6), which is similar to the analytical predictions on the infinite liquid layers by Smith et al. [3].

The critical boundary for the two-dimensional temperature and velocity disturbance which is a special type of the three-dimensional disturbances is also shown in Table 2. The critical Reynolds number Re_{c0} is slightly larger than that for the three-dimensional disturbances except in the range of small aspect ratios (see Figure 4). Figure 7 shows the distributions of the critical two-dimensional temperature and velocity disturbances for the liquid layers of different aspect ratios. For the large aspect-ratio liquid layer, the two-dimensional disturbance mainly develops in the central region and behaves as a wave traveling from the cold region to the hot region. For the small aspect-ratio liquid layer, Γ=3 for instance, the disturbance oscillates with a much higher frequency. Note that for the liquid layer of Γ=3, the critical three-dimensional disturbance as a traveling wave in the spanwise direction, is not allowed in the linear stability analysis with the two-dimensional disturbance. Therefore, the two-dimensional oscillatory disturbance occurs at a much larger critical Reynolds number instead. For the long aspect-ratio liquid layers, the critical two-dimensional disturbance is not much different from the case of the three-dimensional disturbance, and Re_{c0} is only slightly larger than Re_c.

2.2 Curved free surface ($\beta \neq 90$)

Effects of the curved free surface on the flow instability in the liquid layer of Γ=6 were studied. The mesh size $N_z \times N_x$ used in this subpart is 61×351. Figure 8 shows the streamlines and isothermals of the two-dimensional steady flow at the critical states for different contact angles. For the liquid layer with a small contact angle, the concave free surface only allows the liquid thickness in the central region less than unity (see Figure 8a) which restricts the weaker vortex near the cold end. For the liquid layer with a large contact

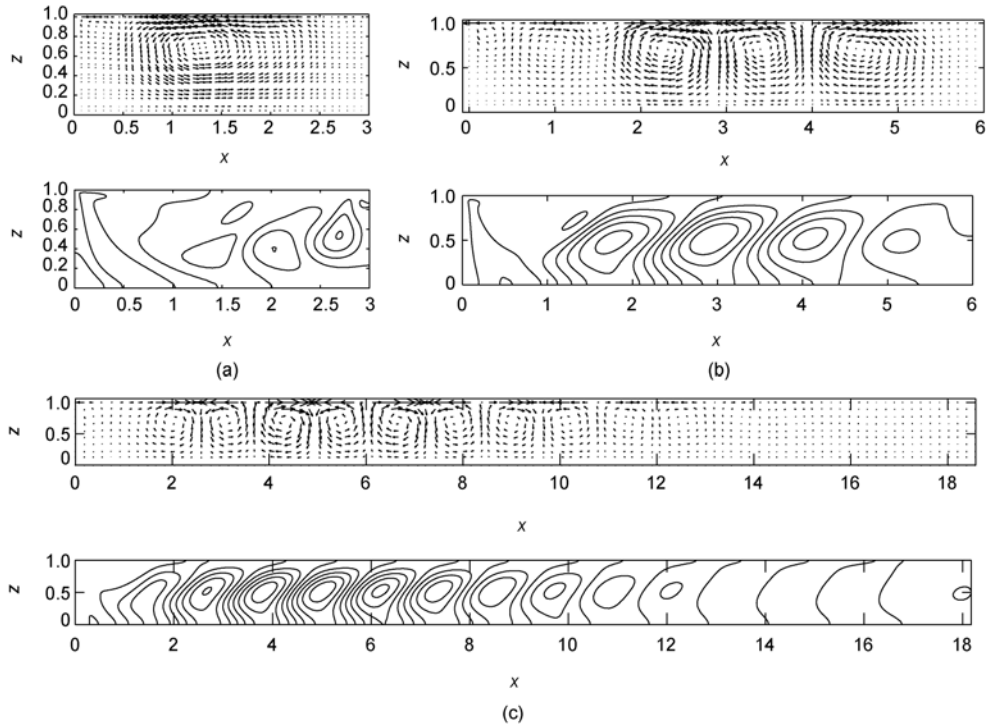

Figure 7 The critical two-dimensional velocity and temperature disturbance distribution. (a) Γ=3, Re_c=356; (b) Γ=6, Re_c=87; (c) Γ=18.6, Re_c=38.

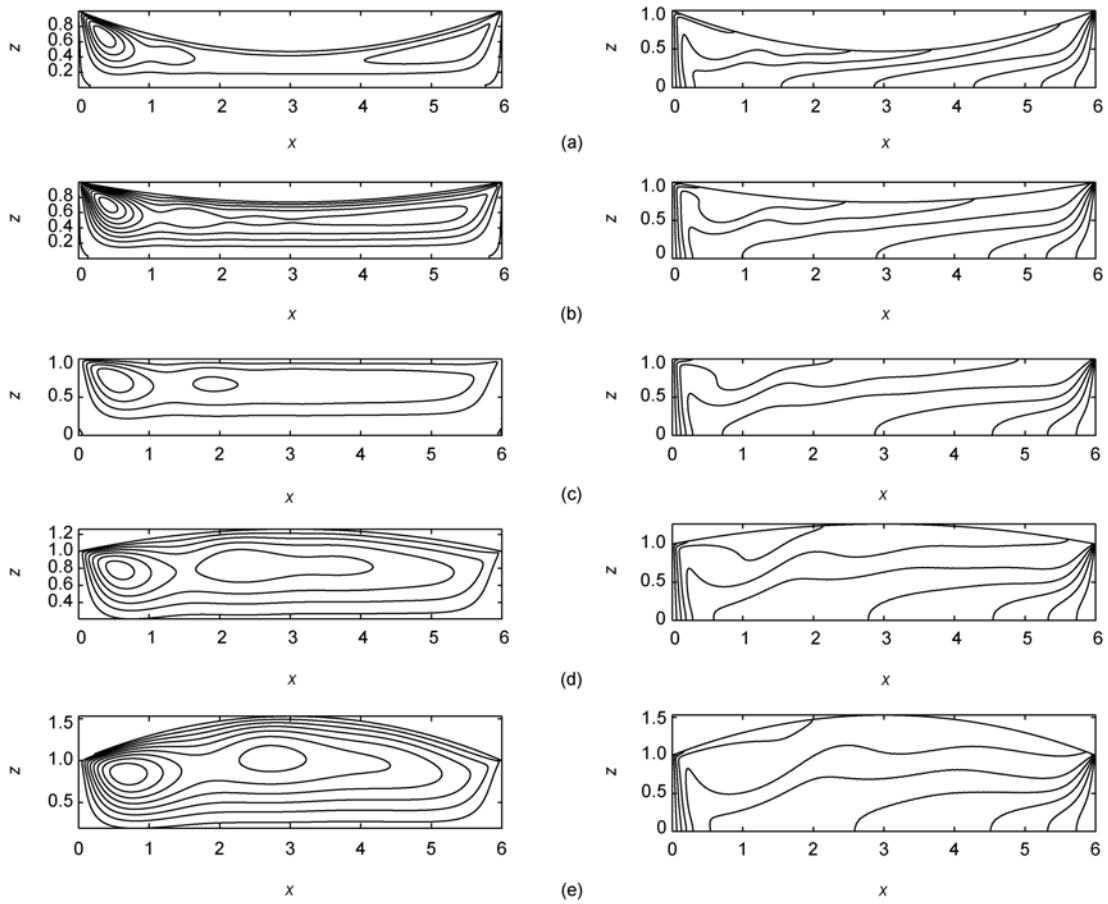

Figure 8 Streamlines and isothermals of the two-dimensional steady basic flow state at the corresponding critical Reynolds number. (a) β=70, Re_c=179; (b) β=80, Re_c=113; (c) β=90, Re_c=82.3; (d) β=100, Re_c=70.7; (e) β=110, Re_c=62.3.

angle, the convex free surface allows the liquid thickness in the central region larger than unity. With the decreasing "effective" aspect ratio, the basic flow state is similar to the small aspect-ratio liquid layer with a flat free surface, Γ=3 for instance.

Table 3 shows the critical Reynolds number Re_c versus the contact angle β. The Re_c decreases with the increasing contact angle β (see Figure 9). The critical wave number and frequency also decreases with an increasing contact angle. Note that with the increasing contact angle, the liquid thickness in the central region increases. In other words, the "effective" aspect ratio decreasing. Figure 10 shows the distributions of the critical three-dimensional disturbance on the free surface of the liquid layers with different contact angles. The critical three-dimensional disturbance in the central region for liquid layers with different contact angles

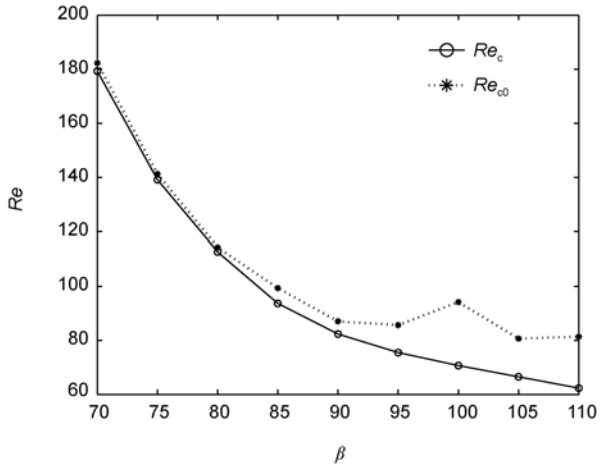

Figure 9 Critical Reynolds number versus contact angle for the liquid layer of Γ=6.

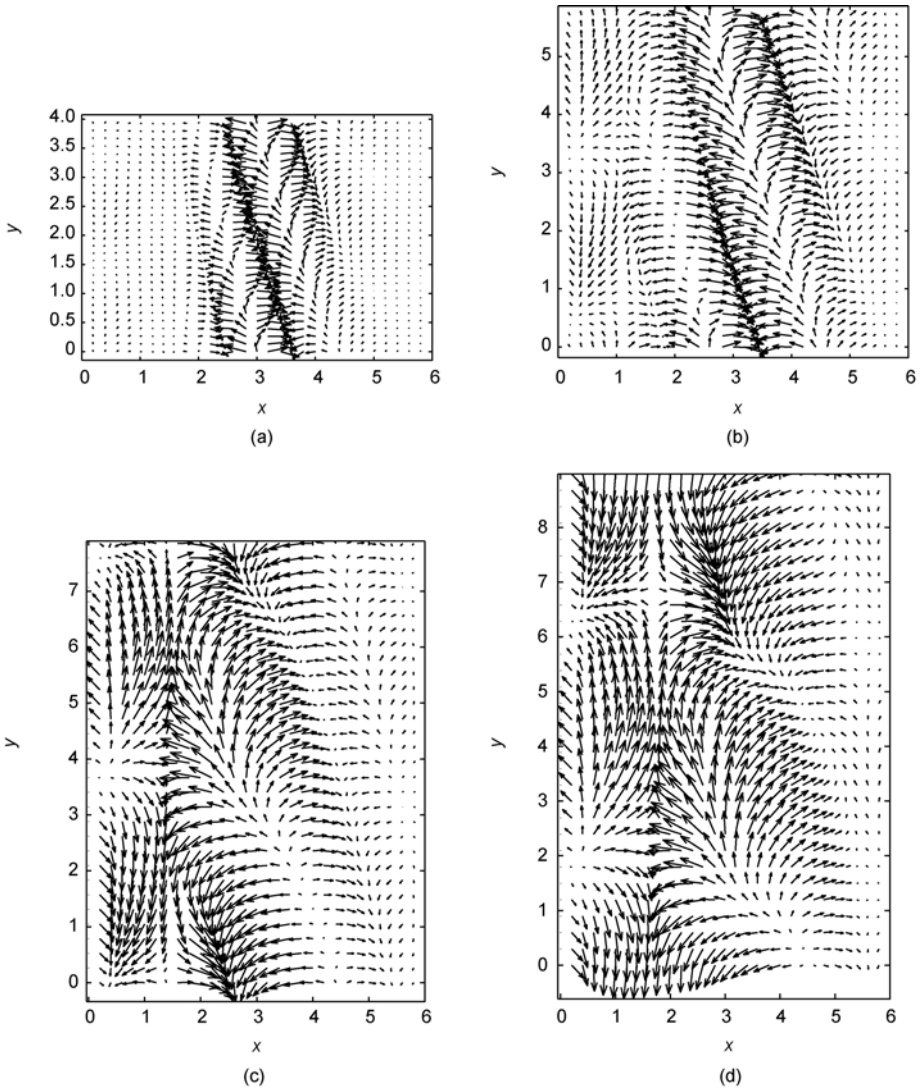

Figure 10 Critical velocity disturbance distribution on the free surface. (a) β=70, Re_c=179; (b) β=80, Re_c=113; (c) β=100, Re_c=70.7; (d) β=110, Re_c=62.3.

is similar, which behaves as an obliquely traveling wave from the cold region to the hot region, and the angle between the traveling direction of the wave and the negative x direction is small. The critical disturbance is different near both ends for liquid layers with different contact angles. For the liquid layer with a concave free surface, the disturbance near both ends is much weaker than that in the central region. For the liquid layer with a convex free surface, the disturbance develops in the whole liquid region. In detail, the obliquely traveling wave in the central region developed into the region near the cold end, and a traveling wave in the spanwise direction is developed near the hot end.

As shown in Figure 9, the critical Reynolds number for the two-dimensional disturbance is slightly larger than that for three-dimensional disturbance, especially in the range of small contact angles. Figure 11 shows the critical two-dimensional velocity disturbance which is a traveling wave from the cold region to the hot region. The disturbance mainly develops in the central region of the liquid layers with concave free surface, and in the whole region of the

Table 3 Critical Reynolds number for a liquid layer of Γ=6 with a different contact angle β

β	Re_c	m_c	f_c	Re_{c0}	f_{c0}
70	179	1.6	12.8	182	12.2
75	139	1.2	7.71	141	7.36
80	113	1.1	5.23	114	4.95
85	93.7	1.2	3.92	99.3	3.63
90	82.3	1.1	3.05	87.0	2.77
95	75.5	0.9	2.40	85.7	2.26
100	70.7	0.8	1.96	94.2	1.75
105	66.5	0.7	1.61	80.7	1.44
110	62.3	0.7	1.40	81.3	1.25

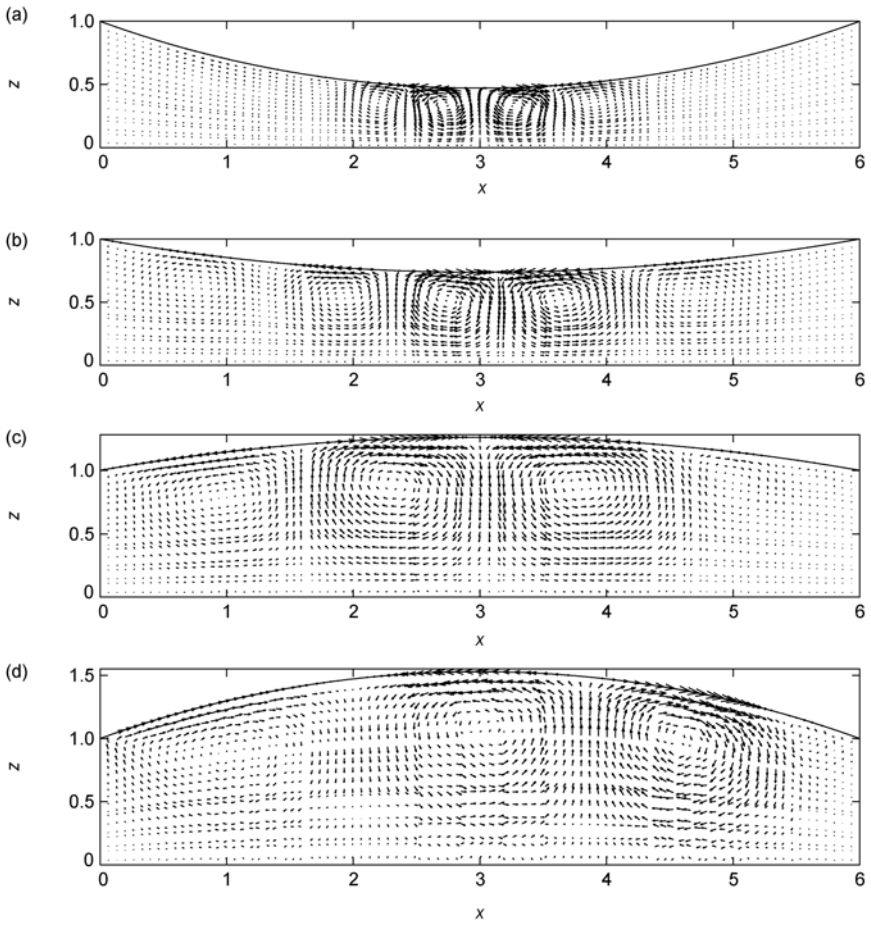

Figure 11 Critical two-dimensional velocity disturbance distribution. (a) β=70, Re_c=182; (b) β=80, Re_c=114; (c) β=100, Re_c=94.2; (d) β=110, Re_c=81.3.

liquid layers with convex free surface. For liquid layer with convex free surface, the traveling wave in the spanwise direction near the hot end which developed in the critical three-dimensional disturbance is not allowed in the two-dimensional analysis, and the corresponding critical Reynolds number of the two-dimensional analysis is larger than that for the three-dimensional analysis.

3 Conclusions

Linear stability of the thermocapillary flow in liquid layers is studied in the present paper, and the critical states for the two- and three-dimensional disturbances are determined. The effects of aspect ratio and the free surface shape of the liquid layer are also studied.

For the liquid layers of different aspect ratios, the critical Reynolds number decreases with the increasing aspect ratio. For the liquid layers of small aspect ratio, the critical disturbance distribution is a traveling wave in the spanwise direction, or an oscillation with a relatively high frequency if restricted to two-dimensional disturbances. For large aspect-ratio liquid layers, the critical disturbance distribution behaves as a traveling wave in the spanwise direction near the hot end and an obliquely traveling wave from the cold end to the hot end in the remaining region. For very long liquid layers, the region near the cold end remains nearly steady with much smaller disturbance compared with the remaining region of the liquid layers.

For liquid layers with a curved free surface, the critical Reynolds number decreases with the increasing contact angle. The critical disturbance in the central region is similar for liquid layers with different contact angles, which is an obliquely traveling wave from the cold region toward the hot region with a small angle between the traveling direction and the negative x direction. The disturbance develops in the whole liquid region in liquid layers with a convex free surface, and with much weaker disturbance near both ends in liquid layers with a concave free surface.

This work was supported by the National Natural Science Foundation of China (Grants No. 10872202 and 11032011).

1 Davis S H. Thermocapillary instabilities. Anu Rev Fluid Mech, 1987, 19: 403–435
2 Schatz M F, Neitzel G P. Experiments on thermocapillary instability. Anu Rev Fluid Mech, 2001, 33: 93–129
3 Smith M K, Davis S H. Instabilities of dynamic thermocapillary liquid layers. Part 1: Convective instabilities. J Fluid Mech, 1983, 132: 119–144
4 Smith M K. Instability mechanisms in dynamic thermocapillary liquid layers. Phys Fluids, 1986, 29: 3182–3186
5 Smith M K. The nonlinear stability of dynamic thermocapillary liquid layers. J Fluid Mech, 1988, 194: 391–415
6 Strani M, Piva R, Graziani G. Thermocapillary convection in a rectangular cavity: asymptotic and numerical simulation. J Fluid Mech, 1983, 130: 347–376
7 Carpenter M, Homsy G M. High marangoni number convection in a square cavity: Part II. Phys Fluids, 1990, A2: 137–149
8 Peltier L J, Biringen S. Time-dependent thermocapillary convection in a rectangular cavity: numerical results for a moderate Prandtl number fluid. J Fluid Mech, 1993, 257: 339–357
9 Saβ V, Kuhlmann H C, Rath H J. Investigation of three-dimensional thermocapillary convection in a cubic container by a multi-grid method. Int J Heat Mass Transfer, 1996, 39: 603–613
10 Lappa M. On the nature and structure of possible three-dimensional steady flows in closed and open parallelepipedic and cubical containers under different heating conditions and driving forces. Fluid Dyn Mater Proc, 2005, 1: 1–19
11 Babu V, Korpela S A. Three-dimensional thermocapillary convection in a cavity. Comput Fluids, 1990, 18: 229–238
12 Xu J, Zebib A. Oscillatory two- and three-dimensional thermocapillary convection. J Fluid Mech, 1998, 364: 187–209
13 Schimmel F, Albensoeder S, Kuhlmann H. Stability of thermocapillary-driven flow in rectangular cavities. Proc Appl Math Mech, 2005, 5: 583–584
14 Golub G H, Van Loan C F. Matrix Computation. Baltimore: Johns Hopkins University Press, 1996